Journal Name

ARTICLE TYPE

Cite this: DOI: 00.0000/xxxxxxxxxx

Supplementary Information: Decoding Magnetization and Magnetic anisotropy in Core@Shell Ferrite Nanoparticles: Interplay between cation distribution and spin disorder†

Rafael Cabreira Gomes,*[a] Vanessa Pilati,[b,c], Fernando Henrique Martins,[c,d], Franciscarlos Gomes da Silva,[c,e], Guilherme Gomide,[c], Bárbara C. C. Pereira,[c], Priscilla Coppola,[f], Fabio Luis de Oliveira Paula,[c], Alex Fabiano Cortez Campos,[f,g], Cynara Kern Barreto,[f,g], Gerardo F. Goya,[h], Florence Porcher,[i,j], Renata Aquino,[f,g], Emmanuelle Dubois,[e], Régine Perzynski,[e] and Jérôme Depeyrot*[c,g]

1 Chemical Synthesis and Sample Preparation

The synthesis of magnetic fluids, as investigated in this study, has been extensively detailed in previous literature[1–3]. The three groups of samples for this paper are colloidal dispersions of magnetic nanoparticles based on Mn-ferrite, Zn-ferrite and Mn-Zn mixed ferrites. These MNPs samples are coated with a maghemite (γ-Fe_2O_3) layer.

The synthesis process of studied nanoparticles and their water based colloidal dispersions which are electrostatically stabilized, follows a three steps procedure.

The first step consists in the simultaneous coprecipitation of metals solutions in alkaline medium. Each group of samples has its appropriate set of resources, as,

- Manganese ferrite: polycondensation of solutions of $FeCl_3$ (1 mol/L) and $MnCl_2$ (0.5 mol/L) in methylamine CH_3NH_2 at 100 °C, under vigorous stirring[4].
- Zinc ferrite: polycondensation of $FeCl_3$ (1 mol/L) and $ZnCl_2$ (0.5 mol/L) in a NaOH (1 mol/L) at 100 °C in vigorous stirring.
- Mixed ferrite: prepared also by hydrothermal coprecipitation of aqueous solutions of Fe^{3+} (1 mol/L), Zn^{2+} (0.5 mol/L), and Mn^{2+} (0.5 mol/L) in NaOH (2 mol/L) at 100 °C in vigorous stirring. Aiming a stoichiometric composition of mixed ferrite core ($Zn_\delta Mn_{(1-\delta)}Fe_2O_4$, the metallic salt mixtures Zn:Mn:Fe are tuned as δ:(1-δ):2 (with δ varying between 0.1 and 0.9). Detailed descriptions of these syntheses are available in the cited literature[5].

The resulting precipitate was magnetically decanted and washed with distilled water. Afterward, the MNPs are then cleaned with 2 mol/L of HNO_3, effectively reversing the surface charge of the nanoparticles and removing possible undesirable by-products.

Secondly, the core@shell morphology is achieved from a surface treatment. Hydrothermal treatment with an iron (III) nitrate solution ($Fe(NO_3)_3$ - 1 M) for 15 minutes at 100 °C, creates an iron rich surface (γ-Fe_2O_3 shell). This maghemite shell protects the ferrite core from acidic dissolution and should modulate the MNPs magnetic properties. All investigated samples here were submitted to that treatment.

Finally, the MNPs are peptized in acidic medium (HNO_3) by adjustment of the pH which establishes the surface charge density and of the ionic strength which screens the MNPs surface potential in water. This strategy leads to an electric double layer that prevents

[a] Departamento de Física, Universidade Federal de Santa Catarina, 88040-900, Florianópolis, SC, Brazil; E-mail: r.cabreira.gomes@ufsc.br
[b] Department of Physics, University of Oviedo, Campus de Viesques, 33204 Gijón, Spain
[c] Complex Fluids Group, Instituto de Física, Universidade de Brasília, Caixa Postal 04455, 70919-970, Brasília, DF, Brazil; E-mail: jerome@unb.br
[d] Instituto de Ciência Tecnologia e Inovação, Universidade Federal da Bahia, UFBA, 42809-000, Camaçari, Brazil
[e] Sorbonne Université, CNRS, PHysico-chimie des Electrolytes et Nanosystémes InterfaciauX, F-75005, Paris, France
[f] Laboratory for Environmental and Applied Nanoscience - LNAA, Faculdade UnB Planaltina, Universidade de Brasília, 73345-010, Brasília, DF, Brazil
[g] International Center of Physics, Institute of Physics, Univ. of Brasilia, 70910-900 Brasília, DF, Brazil
[h] Instituto de Nanociencia y Materiales de Aragón (INMA), Universidad de Zaragoza, Zaragoza, Spain
[i] Laboratoire Léon Brillouin UMR 12 CEA/CNRS Bâtiment 563, Centre d ´Etudes Nucléaires CEA/Saclay, 91191 Gif-sur-Yvette Cedex, France
[j] European Spallation Source ERIC (ESS), P.O. Box 176, SE-22100 Lund, Sweden

agglomeration of nanoparticles.

The mean diameter of MNPs may be attained acting on the rate of mixing of the reagents, temperature, reagent concentrations, and stirring rate. The mean diameter of Zn-ferrite MNPs is tuned by varying the addition rate of the reagents, maintaining constant the other parameters[6]. In the case of Mn-ferrite samples, the mean diameter is tuned by varying the pH of alkaline medium[7].

2 Neutron Powder Diffraction data analysis

To extract the quantitative data from the NPD spectra we have performed the Rietveld refinement using GSAS© package. In brief words, a Pseudo-Voigt function was used which includes a correction for peak asymmetry and a background intensity. Each iteration is fitted until convergence, reached when the reliability factor of refinement R_{wp} and quality of fit χ^2_R are below the critical levels accepted[8].

Two phases are considered, one crystallographic with a spatial group Fd3m associated with the non-stoichiometric ferrite structure, which produces vacancies in the crystal, and one magnetic related to the spatial group F1[9,10]. We use the F1 magnetic structure to circumvent a difficulty encountered when using the GSAS program, which does not allow to enter data from magnetic moments for the Fd3m spatial group. Otherwise, we could refine together both the chemical phase and the magnetic phase considering a single phase with the same spatial group. We performed the refinement considering the magnetic structure F1, with the spins oriented along the z-axis in ferrimagnetic order between A and B sites, because using this spatial group, we could insert the magnetic moments for the cations of Mn, Zn and Fe and obtain the diffraction peaks observed in the experimental data, although this space group has less symmetry operations.

The ionic positions of spinel crystalline structure are taken from the international tables of crystallography[11] by assuming the chemical composition of sample's core.

Finally, the refinements are obtained by taking some free parameters such as the background intensity, the cubic cell size, diameter of MNPs, cation distribution, the oxygen position and oxygen vacancies, the isotropic thermal parameter and the net magnetic moments of $A-$ and $B-$ sites.

3 Samples and protocols of magnetic measurements

The samples were prepared in an homemade sample holder composed by a tube of 50 mm^3 and a stopper of plexyglass. After filling the sample holder with the ferrofluid, the stopper was adhered to the tube with chloroform. That sample holder had its magnetic properties measured in both manners: empty and filled with distilled water. Such paramagnetic/diamagnetic resulting signal of sample holder was used as a blank signal.

The main magnetic measurements were performed using a Quantum Design PPMS Mod. 6000 with VSM setup. That apparatus is equipped with a superconducting coil which produces magnetic fields in the range of ± 9 T in temperatures from 350 K until 2 K.

Magnetic field dependence of magnetization (M×H) of samples was measured at 300 K and 5 K. The latter was performed in Zero Field Cooling (ZFC) procedure, where the measure was recorded after freezing the sample in null external magnetic field.

4 Core@shell model

After hydrothermal surface treatment, a superficial layer of maghemite is formed on the ferrite core. The volume fraction of the core (Φ_C) is then proportional to the content of divalent metal M^{2+}, which is here Mn, Zn, or Mn + Zn. On the other hand, the volume fraction of the layer (Φ_s) is proportional to the iron content of the shell. The volume fraction of the whole particle is expressed as, $\Phi = \Phi_c + \Phi_s$, where:

$$\Phi_c = [M^{2+}]V^{core} \quad (1)$$

$$\Phi_S = \frac{1}{2}\left[([Fe^{3+}] - \frac{\varepsilon}{\alpha+\beta}[M^{2+}])\right]V^{shell}, \quad (2)$$

being the coefficients V^{core} and V^{shell}, the molar volumes of the core and shell, respectively. Then, the determination of the volume fraction of each phase is obtained from chemical measurements of metallic cations.

5 Details of magnetic anisotropies determination

To obtain the effective magnetic anisotropy (κ_{eff}) of core@shell nanoparticles and additional contributions we have used the methodology presented in JALCOM, 824, 153646 (2020). The magnetic anisotropy of the core (κ_C^{exp}) was obtained from the relation,

$$H_C = 0.48\frac{2\kappa_{\text{C}}^{exp}}{\mu_0 m_{\text{S}}} \quad (3)$$

being μ_0 the magnetic permeability of vacuum and M_{irr} is the magnetization where the two branches of hysteresis loops are crossed. According to that methodology, this point is considered as the saturation magnetization of the nanoparticle assembly.

The effective anisotropy (κ_{eff}) of core@shell nanoparticles was obtained from,

$$H_{\text{irr}} = \frac{2\,\kappa_{\text{eff}}}{\mu_0 M_{\text{irr}}} \tag{4}$$

being H_{irr} the magnetic field where the two branches of hysteresis loops are crossed, also named in the literature as closure field. The values used in that procedure are showed below.

Table 1 Magnetic properties of different materials.

	H_c (kA/m)	m_s (kA/m)	H_{irr} (kA/m)	M_{irr} (kA/m)	κ_C^{exp} (J/m^3)	κ_{eff} (J/m^3)
Mn1	22.7	515	1060	365	1.08×10^4	2.43×10^5
ZM3	23.0	452	340	422	1.26×10^4	9.02×10^4
ZM6	21.4	520	322	456	1.27×10^4	9.20×10^4
ZM9	24.5	468	480	454	1.45×10^4	1.37×10^5
Zn1	10.3	368	159	298	4.00×10^3	2.97×10^4

6 Details of calculation of saturation magnetization

To calculate the saturation magnetization of core@shell nanoparticles, we have used the model written below,

$$m_S^{core} = \frac{\rho^{[core]} N_A}{M_w^{[core]}} \left[\sum n_{[B]} - \sum n_{[A]}\right] \mu_B \tag{5}$$

being N_A the Avogadro number, μ_B the Bohr Magneton, $\rho^{[core]}$ and $M_w^{[core]}$ are the nanoparticle core's density (g/cm3) and molecular mass (g/mol), respectively. Finally, $\sum n_A$ and $\sum n_B$ are the quantity of Bohr magneton in the crystalline structure of the spinel tetrahedrical (A site) and octahedrical (B site), respectively.

Starting from the calculation of the molecular mass of the ferrite cores, we obtain $M_w^{[core]}$ using the tabulated molar mass of the cations such as Zn = 65.37 g/mol; Fe = 55.85 g/mol; Mn = 54.94 g/mol and O = 16 g/mol, weighted by the cationic distribution of the samples, as described in the table below.

Table 2 Summary of values used in the calculation of saturation magnetization of magnetic nanoparticles' core. The columns are: investigated samples, chemical composition, molecular mass ($M_{w[core]}$), lattice parameter ($\langle a \rangle$), molar volume of spinel crystalline structure ($V_{w[core]}$), density of ferrite ($\rho_{[core]}$) and saturation magnetization of nanoparticles' core ($m_{S[C]}$).

	Chemical composition	$M_w^{[core]}$ g/mol	$\langle a \rangle$ (nm)	$V_w^{[core]}$ (m^3/mol)	$\rho^{[core]}$ (g/cm^3)	m_S^{core} (kA/m)
Mn1	$Mn_{0.89}Fe_{1.78}O_4$	212.31	0.8401	4.460×10^{-5}	4.760	542.18
ZM3	$(Zn_{0.23}Mn_{0.61})Fe_{1.93}O_4$	220.34	0.8391	4.445×10^{-5}	4.956	505.04
ZM6	$(Zn_{0.42}Mn_{0.37})Fe_{2.04}O_4$	225.72	0.8382	4.431×10^{-5}	5.094	552.66
ZM9	$(Zn_{0.62}Mn_{0.10})Fe_{2.16}O_4$	230.67	0.8383	4.433×10^{-5}	5.203	562.19
Zn1	$ZnFe_2O_4$	241.08	0.8411	4.476×10^{-5}	5.386	424.08

The molecular volume of the core's unit cell ($V_w^{[core]}$) of the MNPs was obtained by the mean lattice parameter $\langle a \rangle$ of the spinel crystalline structure. Note in the equation (5) that $m_S^{[core]}$ can be equally obtained using only $V_w^{[core]}$. To go further, the density of the nanoparticle core ($\rho_{([core])}$) was obtained by definition $\rho^{[core]} = M_w^{[core]}/V_w^{[core]}$.

The spin-only magnetic moment in Bohr magnetons into the spinel crystalline A- and B- sites are counted considering the valence of cations. Here we used Zn^{2+}=0 μ_B, Mn^{3+}=3 μ_B (average valence state), Fe^{3+}=5 μ_B. Applying all of these values (presented in the table 2) in Equation (5), we have the saturation magnetization of the nanoparticles core ($m_S^{[core]}$). These results are shown in Table 2.

To consider the influence of maghemite shell on the saturation magnetization of core@shell nanoparticles, we propose the equation (4) of main text, described as,

$$m_S^{MNP} = m_S^{core}\frac{\Phi_C}{\Phi_p} + m_S^{shell}\frac{\Phi_S}{\Phi_p}$$

where m_S^{MNP} is the saturation magnetization of whole core@shell nanoparticle, m_S^{core} and m_S^{shell} are the saturation magnetization of core and shell, respectively. Here we used as m_S^{shell} the saturation magnetization of the maghemite nanoparticles, whose value is equal to 300 kA/m [12]. The variables Φ_C, Φ_S and Φ_p are the volumetric fractions of core, shell and the whole core@shell nanoparticles, respectively. The latter values were experimentally obtained from Flame Atomic Absorption Spectroscopy (FAAS).

Table 3 Values used to calculate the saturation magnetization of core@shell nanoparticles eq.(4). Φ_S/Φ_p is the volumetric fraction of maghemite shell and m_S^{MNP} is the saturation magnetization of core@shell nanoparticles.

	Φ_S/Φ	m_S (kA/m)
Mn1	0.248	494.5
ZM3	0.257	465.2
ZM6	0.279	496.1
ZM9	0.423	472.4
Zn1	0.420	362.9

Table 4 The table presents a summary of the characteristics obtained from the analysis of the FFT images of ZM3 sample. The columns are, respectively: observed crystallographic planes, interplanar spacing of the bulk reference materials, diffraction spot pairs corresponding to the observed crystallographic planes, and the distance calculated from the FFT image.

Cryst. Plane			Fig.1D		Fig.1F		Fig.1G	
	$MnFe_2O_4$ [11] d_{hkl}(nm)	$ZnFe_2O_4$ [11] d_{hkl}(nm)	Diffraction points pairs	Mean distance (nm)	Diffraction points pairs	Mean distance (nm)	Diffraction points pairs	Mean distance (nm)
[111]	0.487	0.491	n.o.	n.o.	9 10	0.476	1 2	0.486
					17 18	0.488	3 4	0.501
					-	-	29 30	0.493
[220]	0.298	0.301	1 2	0.292	7 8	0.295	5 6	0.304
			5 6	0.299	-	-	13 14	0.301
			7 8	0.297	-	-	17 18	0.298
			11 12	0.291	-	-	19 20	0.297
			15 16	0.299	-	-	-	-
[311]	0.254	0.256	3 4	0.252	1 2	0.254	7 8	0.258
			13 14	0.254	3 4	0.251	9 10	0.261
			17 18	0.253	5 6	0.252	21 22	0.257
			-	-	11 12	0.244	23 24	0.248
			-	-	13 14	0.243	25 26	0.253
			-	-	15 16	0.254	27 28	0.249
			-	-	-	-	31 32	0.263
[400]	0.210	0.212	9 10	0.210	n.o.	n.o.	11 12	0.216
			-	-			15 16	0.218

n.o. = not observed

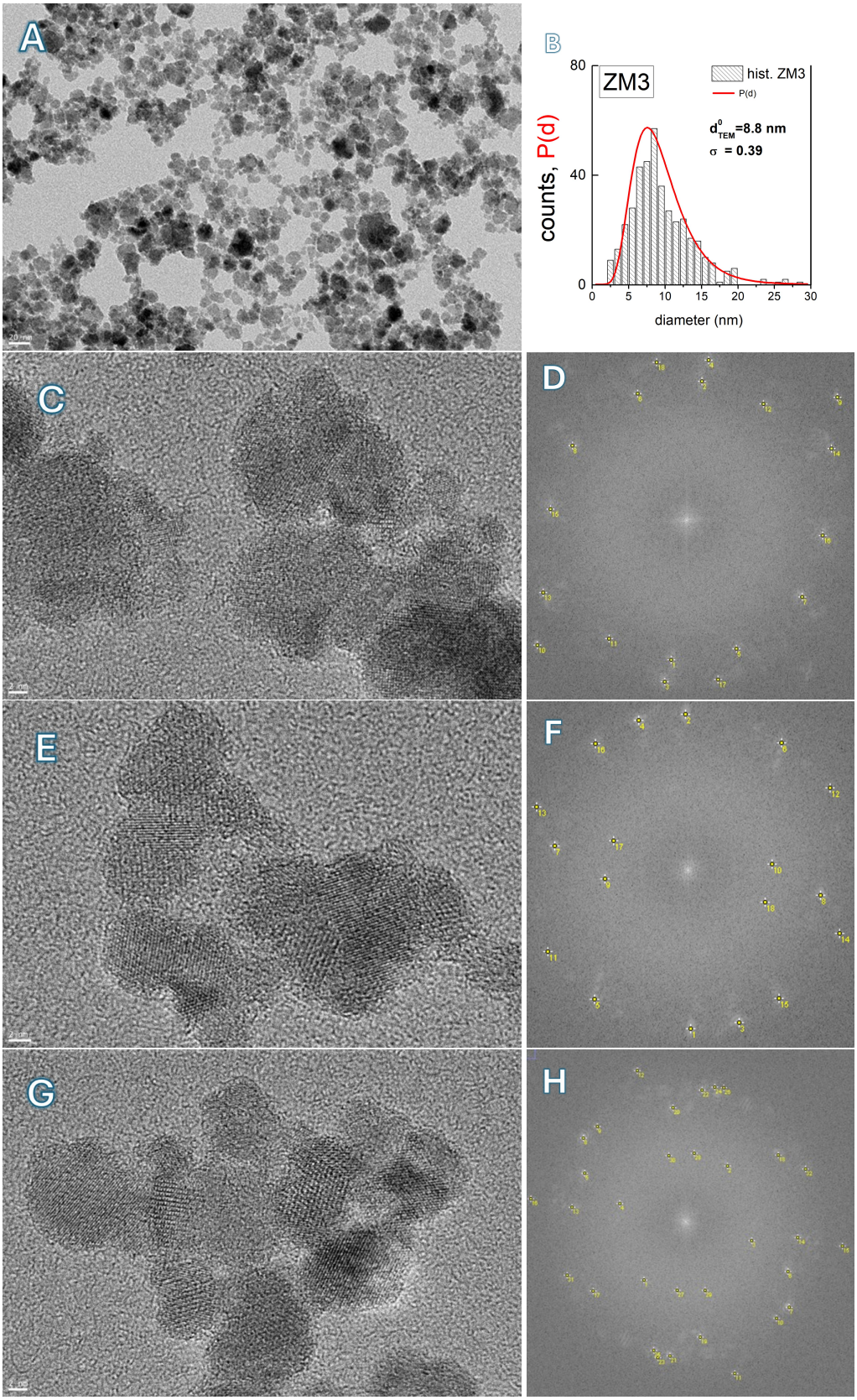

Fig. 1 Microscopic images of sample ZM3 and their respective analyses. A – TEM image; B – log-normal size distribution representative of the sample. Panels C, E, and G are HRTEM images of the sample. Panels D, F, and H show the FFT processing of images C, E, and G, respectively.

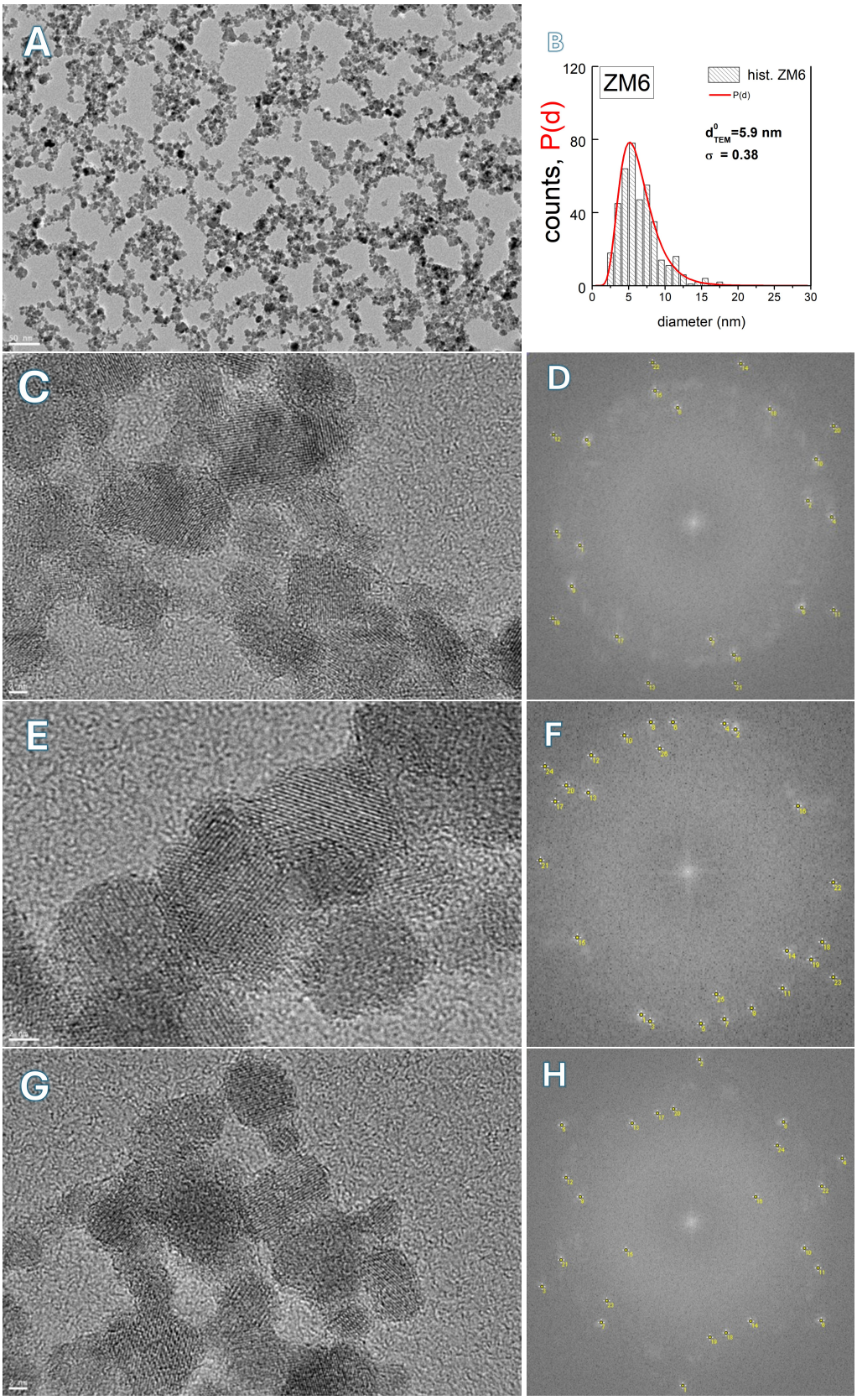

Fig. 2 Microscopic images of sample ZM6 and their respective analyses. A – TEM image; B – log-normal size distribution representative of the sample. Panels C, E, and G are HRTEM images of the sample. Panels D, F, and H show the FFT processing of images C, E, and G, respectively.

Table 5 The table presents a summary of the characteristics obtained from the analysis of the FFT images of ZM6 sample. The columns are, respectively: observed crystallographic planes, interplanar spacing of the bulk reference materials, diffraction spot pairs corresponding to the observed crystallographic planes, and the distance calculated from the FFT image.

Cryst. Plane			Fig.2D		Fig.2F		Fig.2H	
	$MnFe_2O_4$ [11] d_{hkl} (nm)	$ZnFe_2O_4$ [11] d_{hkl} (nm)	Diffraction points pairs	Mean distance (nm)	Diffraction points pairs	Mean distance (nm)	Diffraction points pairs	Mean distance (nm)
[111]	0.487	0.491	n.o.	n.o.	n.o.	n.o.	15 16	0.494
[220]	0.298	0.301	1 2	0.304	13 14	0.298	9 10	0.301
			7 8	0.303	15 16	0.295	13 14	0.300
			-	-	25 26	0.302	17 18	0.301
			-	-	-	-	19 20	0.300
			-	-	-	-	23 24	0.300
[311]	0.254	0.256	3 4	0.256	1 2	0.254	7 8	0.255
			5 6	0.259	3 4	0.251	11 12	0.258
			9 10	0.256	5 6	0.252	21 22	0.255
			15 16	0.257	7 8	0.244	-	-
			17 18	0.258	9 10	0.243	-	-
			-	-	11 12	0.254	-	-
			-	-	17 18	0.251	-	-
			-	-	19 20	0.252	-	-
			-	-	21 22	0.259	-	-
[400]	0.210	0.212	11 12	0.214	23 24	0.213	1 2	0.212
			13 14	0.213	-	-	3 4	0.212
			19 20	0.208	-	-	5 6	0.213
			21 22	0.214	-	-	-	-

n.o. = not observed

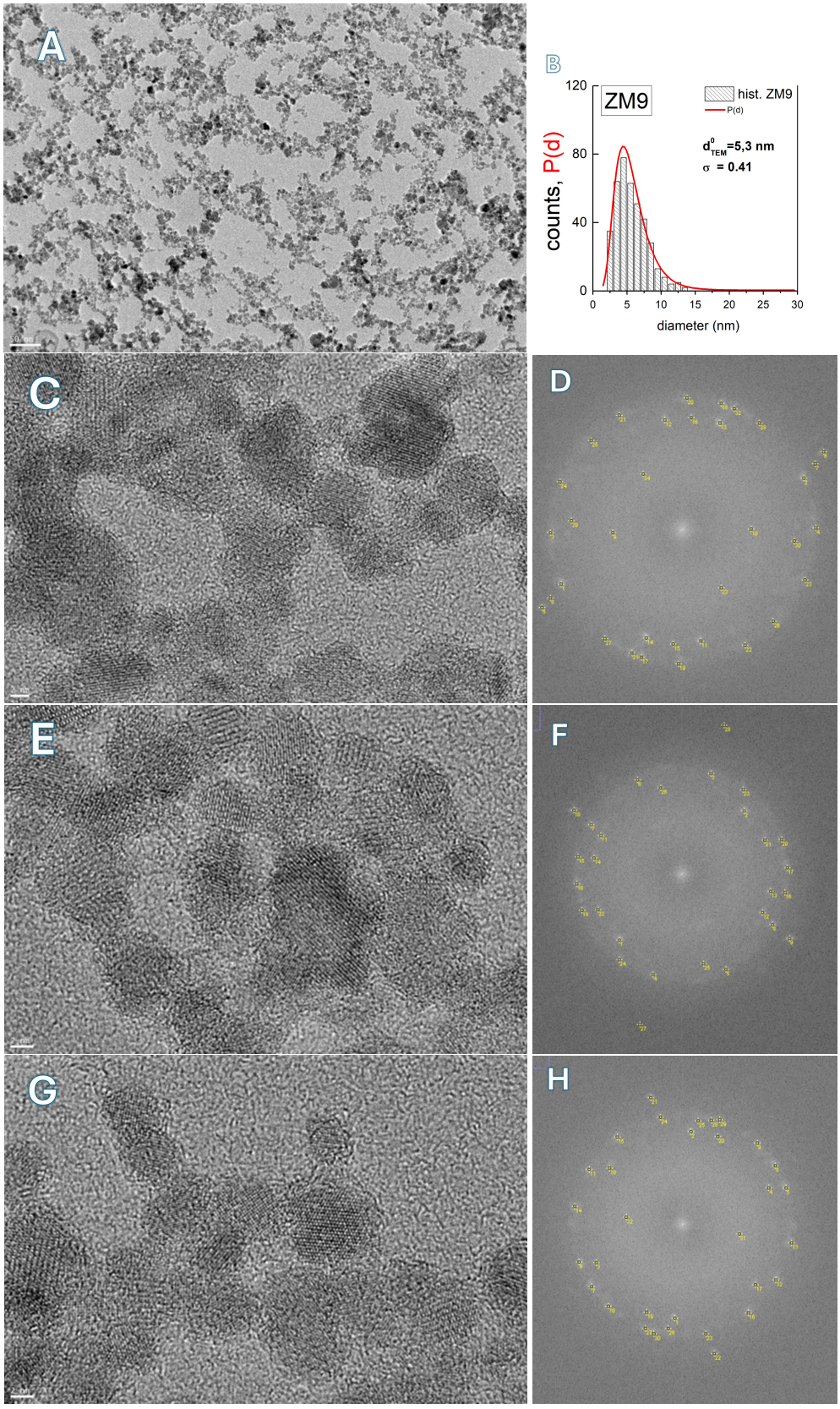

Fig. 3 Microscopic images of sample ZM3 and their respective analyses. A – TEM image; B – log-normal size distribution representative of the sample. Panels C, E, and G are HRTEM images of the sample. Panels D, F, and H show the FFT processing of images C, E, and G, respectively.

Table 6 The table presents a summary of the characteristics obtained from the analysis of the FFT images of ZM9. The columns are, respectively: observed crystallographic planes, interplanar spacing of the bulk reference materials, diffraction spot pairs corresponding to the observed crystallographic planes, and the distance calculated from the FFT image.

Cryst. Plane			Fig.3D		Fig.3F		Fig.3H	
	$MnFe_2O_4$ [11] d_{hkl}(nm)	$ZnFe_2O_4$ [11] d_{hkl}(nm)	Diffraction points pairs	Mean distance (nm)	Diffraction points pairs	Mean distance (nm)	Diffraction points pairs	Mean distance (nm)
[111]	0.487	0.491	9 10	0.491	n.o.	n.o.	31 32	0.485
			33 34	0.493			-	-
[220]	0.298	0.301	11 12	0.303	1 2	0.293	1 2	0.295
			13 14	0.299	11 12	0.294	3 4	0.295
			15 16	0.299	13 14	0.292	17 18	0.297
			29 30	0.304	21 22	0.291	19 20	0.292
			-	-	25 26	0.291	-	-
[311]	0.254	0.256	1 2	0.257	3 4	0.252	5 6	0.252
			3 4	0.256	5 6	0.252	7 8	0.252
			17 18	0.255	7 8	0.254	9 10	0.251
			19 20	0.255	15 16	0.251	11 12	0.255
			21 22	0.259	17 18	0.249	13 14	0.252
			23 24	0.258	19 20	0.248	15 16	0.253
			25 26	0.256	23 24	0.250	23 24	0.250
			27 28	0.256	-	-	25 26	0.264
			31 32	0.256	-	-	27 28	0.254
			-	-	-	-	29 30	0.247
[400]	0.210	0.212	5 6	0.211	9 10	0.210	21 22	0.210
			7 8	0.229	-	-	-	-
[422]	0.172	0.173	n.o.	n.o.	27 28	0.169	n.o.	n.o.

n.o. = not observed

References

1 F. A. Tourinho, R. Franck, R. Massart and R. Perzynski, *Progress in Colloid Polymer Science*, 1989, **79**, 128–134.

2 F. A. Tourinho, J. Depeyrot, G. J. da Silva and M.C.L. Lara, *Brazilian journal of physics*, 1998, **28**, year.

3 J. de A. Gomes, M. H. Sousa, F. A. Tourinho, R. Aquino, G. J. da Silva, J. Depeyrot, E. Dubois, and R. Perzynski, *The Journal of Physical Chemistry C*, 2008, **112**, 6220–6227.

4 F. A. Tourinho, R. Franck and R. Massart, *Journal of Materials Science*, 1990, **25**, 3249–3254.

5 V. Pilati, R. Cabreira Gomes, G. Gomide, P. Coppola, F. G. Silva, F. L. O. Paula, R. Perzynski, G. F. Goya, R. Aquino and J. Depeyrot, *The Journal of Physical Chemistry C*, 2018, **122**, 3028–3038.

6 J. A. Gomes, G. M. Azevedo, J. Depeyrot, J. Mestnik-Filho, F. L. O. Paula, F. A. Tourinho and R. Perzynski, *The Journal of Physical Chemistry C*, 2012, **116**, 24281–24291.

7 R. Aquino, F. A. Tourinho, R. Itri, M. C. F. L. e Lara and J. Depeyrot, *Journal of Magnetism and Magnetic Materials*, 2002, **252**, 23–25.

8 D. Ko, K. Poeppelmeier, D. Kammler, G. Gonzalez, T. Mason, D. Williamson, D. Young and T. Coutts, *Journal of Solid State Chemistry*, 2002, **163**, 259–266.

9 G. Goya, H. Rechenberg, M. Chen and W. Yelon, *Journal of Applied Physics*, 2000, **87**, 8005–8007.

10 D. Litvin, *Acta Crystallographica Section A: Foundations of Crystallography*, 2008, **64**, 419–424.

11 *International Tables for Crystallography*, ed. M. I. Aroyo, International Union of Crystallography, Chester, England, 2016, vol. A.

12 F. G. Silva, J. Depeyrot, Y. L. Raikher, V. I. Stepanov, I. S. Poperechny, R. Aquino, G. Ballon, J. Geshev, E. Dubois and R. Perzynski, *Scientific Reports*, 2021, **11**, 5474 1–10.